Ultrafast Charge Carrier Dynamics of Silver Nanostructures

Author:
Srikrishnaa J
15MS106

Supervisor:
Dr. Kamaraju Natarajan

A thesis submitted in fulfillment of the requirements for the degree of Master of Science

in the

Department of Physical Sciences

Indian Institute of Science Education and Research, Kolkata

June 2020

Declaration of Authorship

I, Srikrishnaa J, declare that this thesis titled, "Ultrafast Charge Carrier Dynamics of Silver Nanostructures" and the work presented in it are my own. I confirm that:

- This work was done wholly or mainly while in candidature for a research degree at this University.
- Where any part of this thesis has previously been submitted for a degree or any other qualification at this University or any other institution, this has been clearly stated.
- Where I have consulted the published work of others, this is always clearly attributed.
- Where I have quoted from the work of others, the source is always given. With the exception of such quotations, this thesis is entirely my own work.
- I have acknowledged all main sources of help.
- Where the thesis is based on work done by myself jointly with others, I have made clear exactly what was done by others and what I have contributed myself.

Srikrishnaa J

CERTIFICATE

This is to certify that the Dissertation entitled "Ultrafast Charge Carrier Dynamics of Silver Nanostructures" is a bona fide record of independent research work done by SRIKRISHNAA J (15MS106) under my super-vision and submitted to IISER Kolkata, in partial fulfilment for the award of the Degree of MASTER OF SCIENCES in PHYSICAL SCIENCE. The work done here is original and has not been submitted so far, in part or full for any degree diploma of any university or institute.

Dr. Kamaraju Natarajan

Assistant Professor

Dept. of Physical Sciences

IISER Kolkata

Abstract

Srikrishnaa J

Ultrafast Charge Carrier Dynamics of Silver Nanostructures

Ultrafast charge carrier dynamics studies in several materials have given important insights into the relaxation dynamics of carriers and possible band structure of the material. These studies have led to the effective utilization of these materials in the real world. Nanostructures are ubiquitous in material sciences due to a high degree of control in the structure during fabrication and their vast scope of applications. At the nanoscale, the charge carrier dynamics vary significantly from the bulk matter counterpart; hence it becomes important to study the ultrafast carrier dynamics of these structures as well. Several studies on metal and semiconductor nanostructures have shown that carrier dynamics are very sensitive to the nanostructure size and shape. This results in a high degree of tunability in the nanostructures for diverse applications. An attempt to study ultrafast carrier dynamics of silver nanowires (AgNW) using pump probe spectroscopy is explained. Numerical simulations of nanoparticle and nanorod pump probe behaviour based on Mie theory and two temperature model were performed. The simulations show that the value of the negative absorption maxima tends to increase when the pump wavelength is decreased and the decay time of the pump probe absorbance signal tends to decrease with pump fluence. Finally, single beam transmitted light microscopy was performed on MoS_2 powder sample.

Acknowledgements

I would like to begin by thanking my supervisor Dr. Kamaraju Natarajan for introducing me to this field and directing me to the right resources from which to learn. I also am grateful to the amount of belief he had in me and the freedom he gave me not just in the context of the lab but also to explore my own interests. I could only hope my next PI is as friendly and easy to approach as you. I would also like to thank my friend and lab mate Simli Mishra for giving me company and helping me out throughout the year with lab and personal life. I extend my gratitude towards my seniors in the Ultrafast THz lab - Mahendra, Vinay, Anjan, and Sowmya without whose guidance in the lab, I would not have been able to learn as much as I have in the past year.

I would like to thank the Government of India for providing me with the INSPIRE scholarship to pursue my love for science. I would like to thank IISER Kolkata and its entire community for providing me a home away from home. It provided me lifelong memories with friends in the "Adda" as well as the "Bhabhi Bansal" groups, all of whom have helped shape me as the person I am today. I am thankful to Meghana for her unconditional love and support throughout my life at IISER, especially during the final year.

I would like to acknowledge my teachers from before joining IISER Kolkata, who were instrumental in shaping my interests. Usha Acharya, Sandy Acharya, Jasmine Acharya, Krishnamurthy sir, and Rabi sir - thank you for always believing in me and for being a constant reminder to myself of the child-like wonder I possessed in classrooms during my schooling years. I hope to one day be at least half as good a teacher as you all were.

Finally, I would like to thank my family, especially Amma and Appa, without whose hard work, sacrifices, love, and undying support, my education would not have been possible. Thank you all for your continued belief in me.

Author's Note

The experiments proposed could not be performed to the full extent, and the data obtained thus far is not meaningful enough to be able to publish them in this thesis report. The simulation that was tried yielded a few results decent enough to be added to this thesis. However, the simulations were last minute effort to save this thesis and there is a huge scope for improvement. I have tried my best to summarize all the essential topics he learned throughout this year via the numerous papers and reference books. Not to mention the invaluable experience I have gained under the supervision of Dr. Kamaraju Natarajan and the other members of the Ultrafast THz group. I hope this thesis could be a useful guide for the person that would carry on with the study on metal nanowires and perform the proposed experiment/improve upon the simulation or just any new intern/master/Ph.D. student of the lab, as I was about a year ago. I would like to wish them all the best.

Contents

To my parents.

Chapter 1

Introduction

Lasers are a source of great fascination for all. A laser demonstration can drum up crowds in science exhibitions and theme parks alike. In the time leading up to the diamond jubilee of their discovery, lasers have had a plethora of applications in human life - facilitating eye surgery, cooling atoms to a screeching halt, and being set props in high grossing sci-fi films and be- ing an alternative for a long stick during presentations. Lasers facilitate research in STEM fields. They continue to be studied and improved upon even today while enabling research in other fields. Lasers light can be emitted continuously (CW) or in a pulsed fashion [1]. The pulse rate of a laser is like the shutter speed of a camera. With faster pulse rates (or shorter pulse durations), scientists have been able to improve the time resolution in their experiments and have been able to observe phenomena that occur at very low timescales. Lasers with pulse repetition rates in the order of megahertz that impinge on a material enable scientists to probe atomic and molecular processes (such as bond formation/breaking and carrier dynamics, to name a few), which take place at very short timescales in the material. A whole new branch of physics called Ultrafast Physics was born. To date, the lowest recorded pulse width is 43 attoseconds [2].

Ultrafast pump probe spectroscopy, fluorescence spectroscopy, and photoluminescence spectroscopy studies were performed on several 2D materials [3] [4], 1D nanowires [5] and 0D quantum dot [6] [7] samples to determine the effects of dimension confinement on the electronic states and the carrier dynamics in the system. These studies suggest that dimension restriction does indeed change the carrier dynamics in the system. Theoretical studies have shown that the deviations of optoelectric properties from bulk matter counterparts were structure-dependent [8] [9]. Hence the morphology of the nanomaterials can be altered to suit the application. As a result of the studies,

several applications of nanowires have popped up in the field of nanophotonics [10], biological sensing and imaging [11] [12] [13], thermoelectrics [14] and nanoelectronics [15].

This thesis describes an attempt to study the ultrafast pump probe spectroscopy of silver nanowires. Chapter 2 describes the basic working of a laser. Chapter 3 contains a description of nanowires and some characteristics of silver nanowires. Chapter 4 describes the basic theory behind the experimental procedure of pump probe spectroscopy. Chapter 5 contains the detailed methods of the numerical simulation of ultrafast pump probe spectroscopy of silver nanoparticles and nanorods and the summary of results from the simulations. Chapter 6 contains a brief description of transmitted light microscopy and results of transmission microscopy performed on MoS_2 powder. Chapter 7 concludes the thesis and suggests leads for future work on nanowires.

Chapter 2

Basics

Laser light is produced through light-matter interaction and enables studies in vast areas of research, including light-matter interaction. The study of electrons and their interactions with electromagnetic radiation is essential for applications in physics and chemistry. In order to understand light-matter interaction, one must start from the basics.

2.1 Absorption, Spontaneous emission and Stimulated emission

Light interaction with an orbital electron produces three types of processes – absorption, spontaneous emission, and stimulated emission [1]. The electrons revolving in atoms exist in different energy levels. For an electron to jump from a lower (ground) level to a higher (excited) level, it must absorb a light photon of frequency stipulated by the Bohr's frequency condition:

$$\Delta E = h\nu, \tag{2.1}$$

where ΔE is the difference in energies between the levels. This process is known as absorption. The excited electron will not stay in the excited state forever. It will eventually try to return to its original state by losing energy. Spontaneous emission is the reverse phenomenon where an electron existing at the higher energy level spontaneously transitions to the ground state without any external influence, followed by the emission of a photon of frequency given by the same relation.

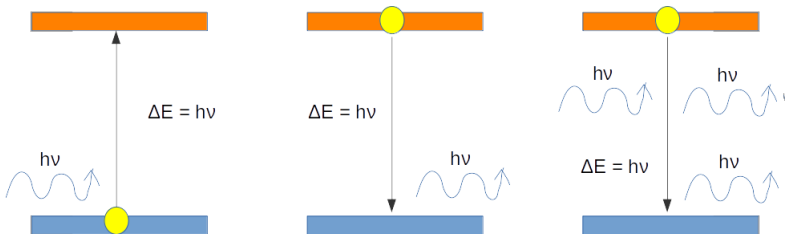

Figure 2.1: Schematic diagrams of absorption, spontaneous emission and stimulated emission respectively.

Stimulated emission is when an electron in the excited state returns to the ground state in the presence of an external electromagnetic field whose frequency corresponds to the energy difference between the states. The photon thus emitted has the same frequency as the external field, phase, polarization, and direction of travel. This process is in contrast to the case of spontaneous emission, where the relaxation of an electron is a random event. Stimulated emission occurs only during "population inversion" - where more atoms in a system are in the excited state than the ground state. By definition, the population inverted state is not the natural state of any system.

An external electromagnetic field can alter the quantum mechanical state of the orbital electron without getting absorbed. As the electron transitions from the excited state to the ground state (which are non-dipole states), it goes through an intermediate dipole state which vibrates at a characteristic frequency. The presence of an external field of the same frequency significantly increases the probability of the electron occupying the intermediate dipole state. Hence, the rate of transition of electrons becomes higher than that of spontaneous emission. Hence this leads to the production of an additional photon of the same frequency, phase, and direction of travel.

2.2 Coherent source of light

Two sources of light are perfectly coherent when they have the same waveform, wavelength, and phase difference between them, throughout [16]. It is a measure of how correlated the waves are as quantified by a cross-correlation. Correlation can be sought for the same wave(self-coherence) at different points in space/time.

Coherence is an essential phenomenon in optics. Many phenomena in optics such as interference, diffraction, holography would not be possible without light coherence. Given the three phenomena mentioned above, stimulated

emission seems to be the only method of coherent light production, and it is indeed how a laser works.

2.3 Laser

2.3.1 Working

Lasers are ubiquitous in optics labs since they are a reliable source of coherent, monochromatic, high-intensity light. A laser typically consists of a cavity, a gain medium, and an energy source for the gain medium [1] as shown in the figure below.

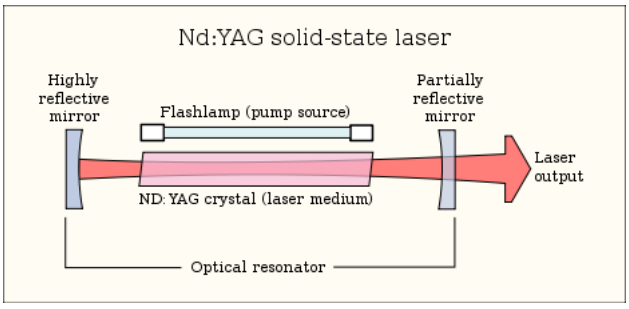

Figure 2.2: Schematic diagram showing the working of a laser. The gain medium here is Nd:YAG which is pumped by a flash lamp so that population inversion is achieved. The light thus produced by stimulated emission bounces back and forth between the mirrors and finds its way out through the partially reflective mirror.

Coherent light in lasers is produced predominantly through the process of stimulated emission. The ejection rate of the photons during stimulated emission depends on the number of atoms in the excited state and the radiation density of the external electromagnetic field. Population inversion does not naturally occur in atomic systems since it is energetically unfavorable to have more atoms in the excited state. Hence, constant pumping of the system that produces the coherent light is essential to ensure population inversion throughout. The energy could be of any form – electrical, chemical, mechanical, or even light from another laser depending on the gain medium. The energy supplied is used to elevate the atoms in the gain medium to the excited state to achieve population inversion.

The gain medium determines the wavelength of the resultant light and its monochromaticity. Different gain media have different wavelengths and spectral widths and hence also categorize lasers into different types - liquid (dye-lasers), solid (Nd:YAG, Ti:Sapphire), gas (He-Ne, Ar) and semiconductor

lasers - to name a few. The gain spectrum of a specific gain medium dictates the wavelength of the output light. Since the light emitted is made to bounce back and forth between the reflecting mirrors, only specific frequency modes of light are allowed. In contrast, the others destructively interfere and are wiped out of the emitted spectrum. These modes are called the cavity modes, and they arise due to the boundary condition imposed by the cavity. The cavity modes are given by:

$$\nu_n = \frac{nc}{2L} \tag{2.2}$$

where n is an integer. The cavity modes which come under the laser envelope are called the laser modes. The emitted laser light will consist of a superposition of all the laser modes.

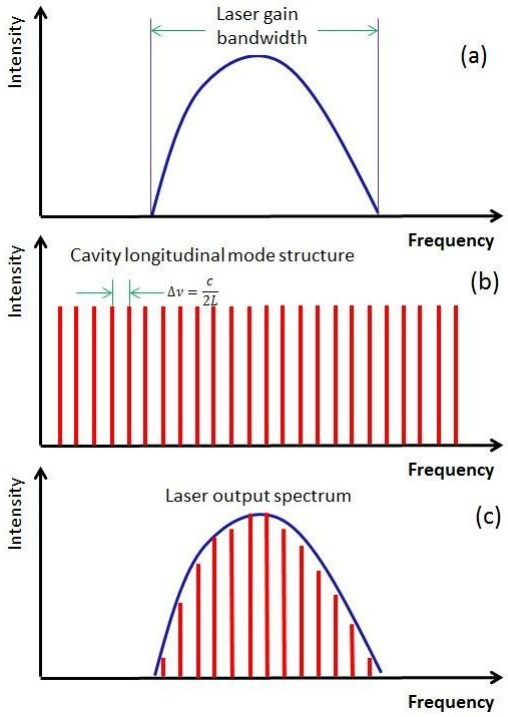

Figure 2.3: Laser modes. The gain spectrum envelope as shown in the first figure. The allowed wavelengths are indicated by discrete, equidistant spikes in the second graph. The spikes which come under the gain spectrum are the laser modes.

2.3.2 Mode Locking

The emitted laser light is a superposition of all the laser modes. These laser modes do not have a well-defined phase relationship with each other. Hence the superposition thus obtained will have beating effects with varying intensity. The introduction of a constant phase relationship between the laser

modes facilitates constructive interference periodically and boosts a specific frequency mode after a short time (pulse repetition time). This process results in the pulsed emission of a bright, monochromatic laser beam. This process is called mode-locking [17]. The number of laser modes governs the pulse width.

$$\Delta t \propto \frac{1}{N\Delta\nu} \tag{2.3}$$

The pulse shape determines the constant of proportionality.

Chapter 3

Nanowires

3.1 Introduction

As the name suggests, nanowires are nano-sized wires with a diameter of hundreds of nanometers and lengths in the order of ones or tens of microns. They are a subclass of nanostructures, which can also be nanoparticles, nanorods, nanosheets, and nanoribbons. Metal (gold, silver) [18] and semiconductor nanowires (Si, ZnO) [5] have been synthesized and studied extensively. Due to size effects, the nanowire's dielectric constant is different from its bulk counterpart, which leads to a variety of exciting, size, and shape-dependent deviations in optical phenomena for the nanostructures [13]. Before getting into the how of these optical studies, it is vital to understand the theoretical understanding of the difference between nanostructures and their bulk counterparts at an atomic level.

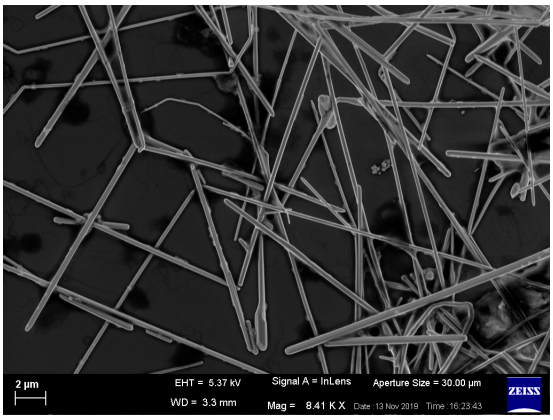

Figure 3.1: Scanning Electron Microscope (SEM) image of silver nanowires obtained from Dr. G. V. Pavan Kumar, IISER Pune. The widths are around 300 nm while the lengths range from 5-25 μ m

3.2 Band Theory

The atomic orbital theory stipulates that there are discrete energy levels an atomic electron can occupy. At the same time, the Pauli Exclusion Principle dictates that only one electron can occupy a given energy level (if we ignore electron spins). In the case of pure solids, a similar theory exists where atomic orbitals of similar energies combine to form continuous energy bands [19] These may be distinguished from one another by gaps present in between them, called forbidden gaps. Electrons within a band roam about freely. However, an electron can jump from a lower band to a higher (not fully occupied) one if the energy supplied to the electron is greater than the gap energy between the bands. The highest energy band that is either wholly or partially occupied by electrons is called the valence band, which is similar to valence shell in atoms.

Meanwhile, the lowest unoccupied band above the valence band is known as the conduction band. The relative positions of the valence and conduction bands in the energy spectrum determine whether the given solid is an insulator, conductor, or a semiconductor. If the gap energy is non-existent, i.e., the two bands overlap, resulting in a partially filled delocalized band, the solid is a conductor. The slightest energy fluctuation can excite the electrons into the conduction band, where they can migrate through the crystal. This may suggest an increase in the conductivity of metals with temperature. In reality, however, it is the opposite. This fact becomes apparent once we account for the increased collision of the excited electrons with the nucleus of the metal atoms. If the gap energy is too high (above 2 eV, say), the solid is an insulator (or a wide band gap semiconductor), and if the gap energy is intermediate, it is a semiconductor. For these materials, an increase in temperature does lead to an increase in conductivity.

The continuous nature of the bulk solids bands results from the theory that the number of resulting orbitals due to bond formation is equal to the the number of atoms that form the bond. The more the number of atoms, the more the number of orbitals of the same energy that combine. Therefore, more the resulting molecular orbitals within a specific span of energy. If the number of combining atoms is very high ($\approx 10^{22}$ for bulk material), the density of resulting orbitals in a band becomes very high, and the energy gap between orbitals in the same band becomes non-existent. Hence the band is considered to be continuous. However, depending on the type of material, there would be clear boundaries between the bands formed by orbitals of

different energy. In the case of conductors, the boundary is non-existent and the bands of different energies overlap. In the case of semiconductors and insulators, the different energy bands have well defined boundaries and are characterized by the forbidden gap energy.

It becomes evident from this explanation that for materials with considerably fewer atoms, this continuous band approximation breaks down, which is precisely the case in mesoscopic and quantum materials. The band structure of quantum dots and 1D/2D materials depends on their size and shape [20] [21]. Naturally, there arises a need to study these unique band structures by observing the trajectory of the electrons and holes throughout excitation and subsequent relaxation processes.

In semiconductor nanowires, spatial confinement increases the direct bandgap [21] [22] and introduces new surface states [23]. Surface plasmons – which are light assisted electron cloud oscillations - were observed to be propagating along the length of the nanowire and even seem to jump nanowires when they are connected end to end, in silver and gold nanowires [24]. Photoluminescence in the visible spectrum has been observed in metal [25] [26] and semiconductor nanowires [27] [28] when impinged with laser light . All of these phenomena shed light on the optical characteristics of nanowires. Hence the band structure and the electron and or hole trajectory can be inferred.

3.3 UV-Vis Spectroscopy

UV-Visible spectroscopy was performed on the silver nanowires to obtain an absorbance versus wavelength relationship.

Using this, a tauc plot to estimate direct band gap was plotted. The fit equation is [29]:

$$(\alpha h\nu)^2 = (h\nu - E_g) \tag{3.1}$$

where α is the absorption coefficient function and E_g is the direct band gap energy. The gap energy for silver nanowires thus obtained is 2.28 eV.

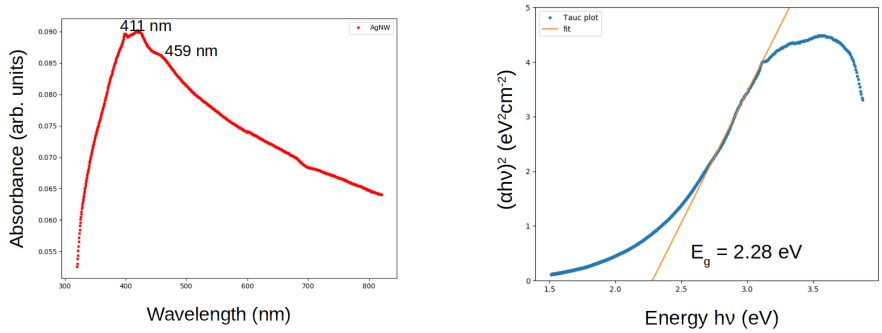

(a) A (b) B

Figure 3.2: A) The UV-Visible absorbance spectroscopy of silvernanowires. A noticeable peak is observed at around 411 nm wave-length. B) The first plot is converted into a Tauc plot and a straightline fit is performed to obtain the true estimate of the band gap insilver nanowires.

3.4 Powder XRD

XRD study was performed on the silver nanowires placed on a glass plate. The figure shows that the overlapping glass background is visible along with sharp peaks that match with the previously reported pattern for silver nanowires [30].

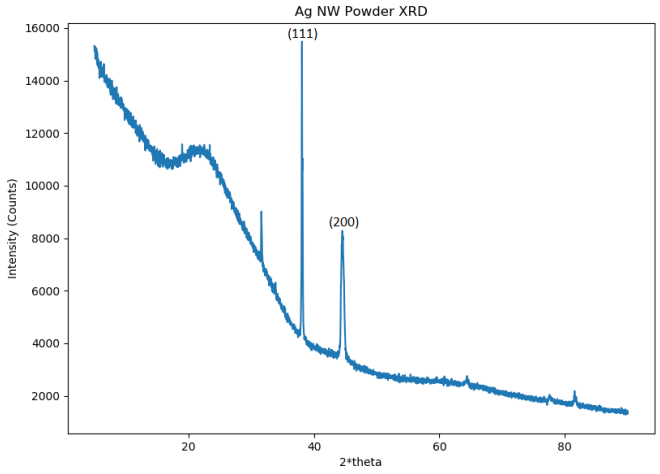

Figure 3.3: Powder XRD data for silver nanowires on a glass slide. An overlapping background is obtained due to the amorphous glass while peaks are obtained due to the silver nanowires. The peaks are found to match with the ones obtained by Junaidi et al.

Chapter 4

Pump Probe Spectroscopy

4.1 Introduction

Light-induced changes in a material are usually obtained by observing the changes in a characteristic of light after impinging upon a sample material. The change is monitored by an avalanche semiconductor photodiode, a very sensitive instrument used to record the intensity of incoming light. The voltage across the diode is proportional to the intensity of incoming light. However, the response time of photodiodes is longer than the timescale of ultrafast processes. Hence to detect changes in the ultrafast timescale, laser light and photodiode alone are not enough. Workarounds such as using streak camera [31], optical Kerr gate [32], up-conversion gate [33], and time-correlated single-photon counting [34] exist, but none more elegant and straightforward than the pump probe spectroscopy.

An ultrafast laser pulse is separated into two – pump and probe. The pump pulse is used to excite the electrons in the sample from the ground to the excited state, which changes the optical properties of the sample, such as complex dielectric constant and refractive index – at that spatial location. The probe pulse (of relatively much lower intensity in order to cause minimum perturbation to the sample), which coincides with the pump pulse spatially but arrives after a controlled time delay, monitors the changes in the optical properties of the sample caused by the pump pulse. The probe pulse may (degenerate) or may not (nondegenerate) be of the same wavelength as the pump. One can study the time evolution of the excited state by varying the time delay between the pump and probe pulses. This technique investigates transmission, reflectivity, Raman scattering, and induced absorption in a sample [5] [35].

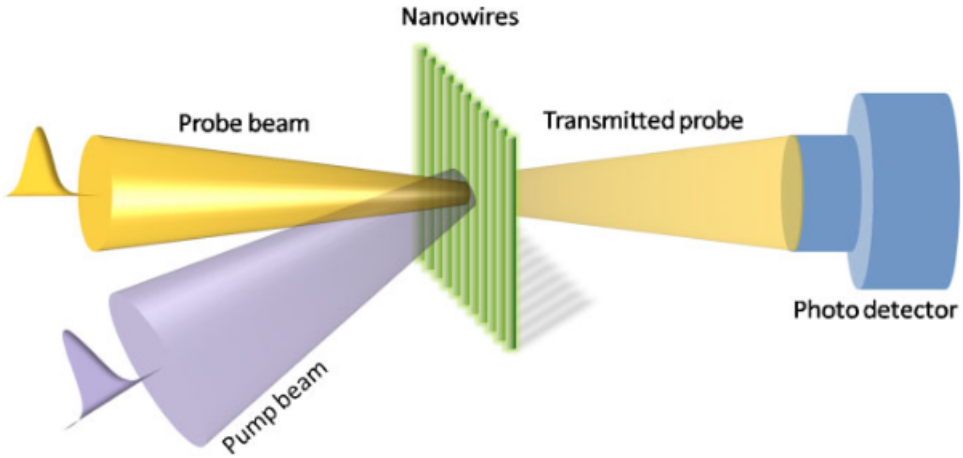

Figure 4.1: Schematic diagram of the pump probe spectroscopy. Differential transmission of probe beam is obtained through this setup. [5]

The main advantage of using pump probe spectroscopy for the study of carrier dynamics is the time resolution control. The temporal resolution limits down to which the carrier dynamics can be probed is only limited by the pulse width. Carrier dynamics have been probed down to resolutions of 24 attoseconds [36] [37].

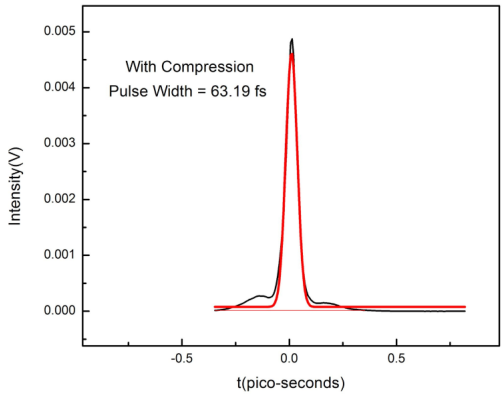

Figure 4.2: Gaussian pulse. Measured cross correlated pulse width is 63 femtoseconds.

4.2 Proposed Setup

The laser used is Coherent Inc. Mantis Ti:Sapphire laser with a peak wavelength at 800 nm and 80 MHz repetition rate. The Fourier transform-limited pulse (of pulse width 35-40 fs and central photon energy 1.57 eV) is divided into two parts using a 90:10 beam splitter. The low power part is used as the

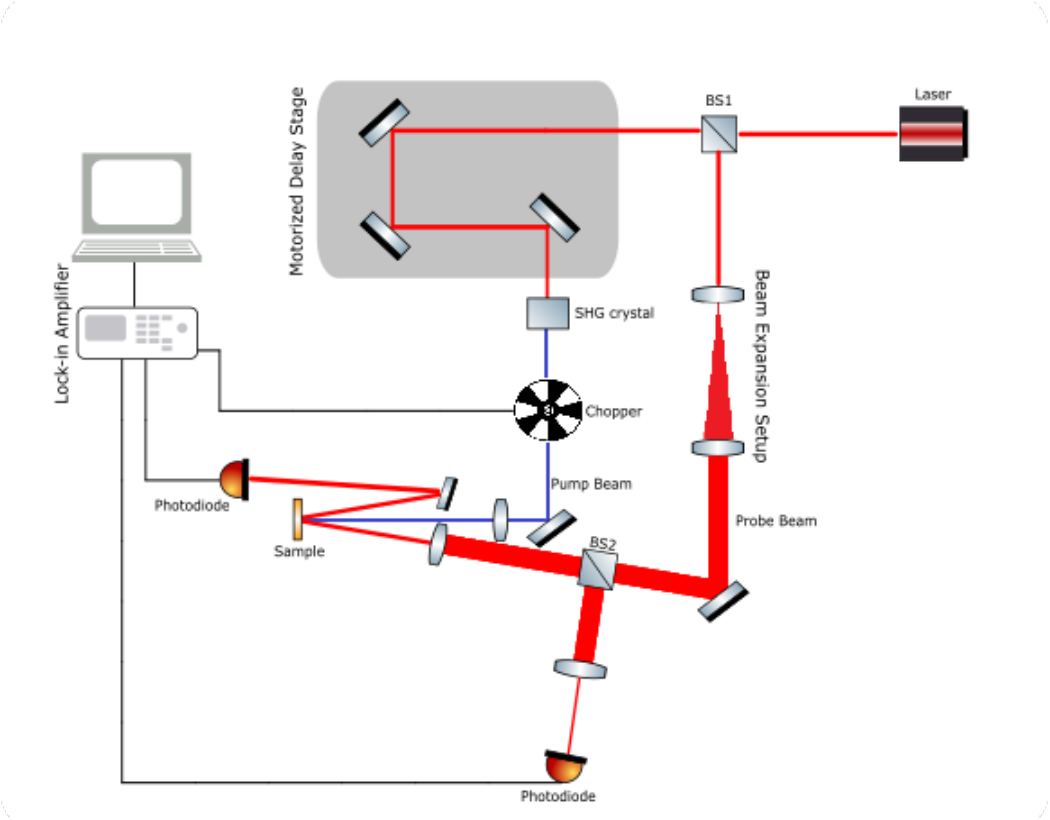

Figure 4.3: The proposed setup for ultrafast pump probe spectroscopy of silver nanowires.

probe while the high power part is used as the pump. The probe beam is then expanded in diameter using two biconvex lenses before being focussed at the sample using a 5X microscope objective. The pump beam goes through a motorized delay stage setup (with 2 mm resolution, which translates to a temporal resolution of 6.6 fs) before being up-converted into a 400 nm beam using a second harmonic generating crystal. A mechanical chopper is placed in the path of the pump beam to subtract the signals arriving from solely the probe and improve the signal to noise ratio of the output. Finally, the pump beam is focussed onto the sample using a biconvex lens. The focal spot diameters ($1/e^2$) were 25 μm and 10μm for pump and probe, respectively.

The reflected probe beam from the sample is focused onto an avalanche photodiode connected to the lock-in amplifier. A reference probe signal (before it impinges on the sample) is connected to the lock-in via a photodiode. The chopper frequency is also fed into the lock-in amplifier. The output signal (ΔR) is the difference between the reference probe (R_0) and the reflected probe signal (R). The differential reflection ($\Delta R/R_0$) is then calculated and plotted as a function of the time delay between the pump and probe beams.

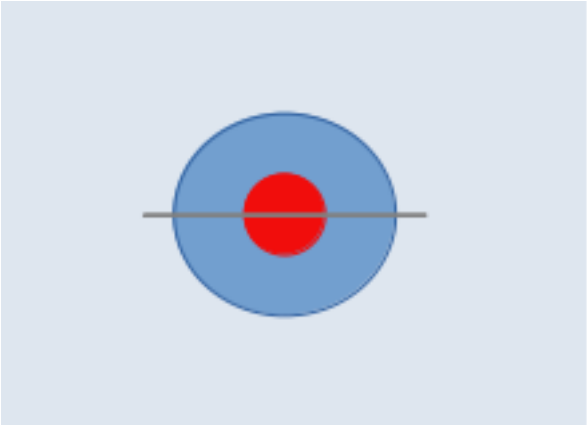

Figure 4.4: Schematic of the pump and probe spots on the nanowire (not drawn to scale). The pump beam is blue in colour while the probe beam is red in colour. The nanowire is depicted as a thin line.

4.3 Theory

The non-degenerate ultrafast pump probe spectroscopy data obtained for α Bismuth Oxide microrods is presented (Figure **??**) for reference. A peak in the differential transmission is observed at zero time delay [29]. The pump excitation energy corresponds to 400 nm wavelength whereas the probe wavelength is 800 nm. Since the gap energy calculated for bismuth oxide microrods is greater than probe energy, the probe beam does not excite electrons from lower to higher energy states. However, at the higher energy band, the probe beam gets absorbed by electrons to reach another state within the band. The probe absorption taking place at the higher energy states is known as photo-induced absorption. This reduces the probe transmission signal obtained from the sample at zero delay.

As the time delay increases, electrons at higher states start losing energy through various processes [5]. Electron-electron thermalization and electron-phonon thermalization are processes where the excited electrons impart their energy to other electrons and the lattice, respectively. This process increases the overall temperature of the electrons and increases the phonon vibration energy. Stimulated emission is, as explained before, a radiative process where excited electrons return to lower states (leading to electron-hole recombination across the band gap) in the presence of an electromagnetic field accompanied by a loss of energy in the form of electromagnetic radiation of the same frequency. This process occurs only while performing degenerate pump probe spectroscopy. Auger recombination is a non-radiative decay process which involves electron-hole recombination across the band gap. The

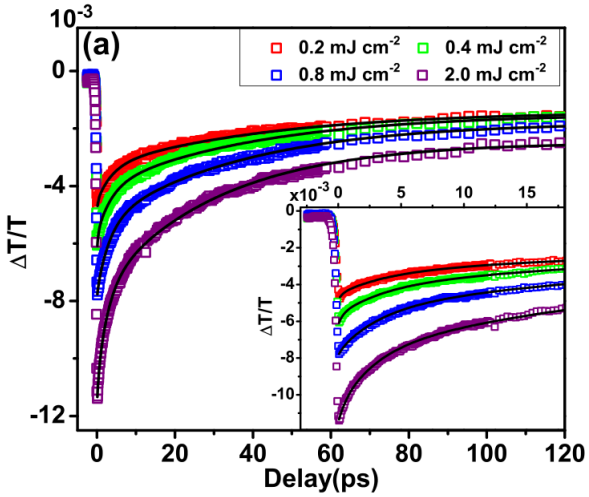

Figure 4.5: Ultrafast pump probe differential transmission spectroscopy of α Bismuth Oxide microrods obtained by Sarkar et al (2019). The study is performed for different pump fluences. The solid black lines are the tri-exponential fit.

energy is transferred to another electron or hole, which is kicked to a higher energy state. The time scales and strengths of the processes depend strongly on the impurities and their concentrations in the sample material, the sample morphology, the pump photon energy, and photoexcitation density.

The following equation can model the decay of differential reflection/transmission with time delay for any material [38]:

$$\frac{\Delta R}{R_0} = (1 - \exp(-t/\tau_r)) \sum_{i=1}^{N} A_i \exp(-t/\tau_i) \tag{4.1}$$

where i sums over the N governing relaxation processes. τ_r denotes the rise time of the signal and corresponds to the thermalization of the photoexcited carriers. A and τ denote the amplitude and the timescale of the processes.

After the completion of one run, the fluence (energy per unit area) of the pump beam is changed, and the subsequent changes in the differential reflection of the probe as a function of the time delay recorded. Increasing the fluence of the pump beam increases the energy of the laser spot per unit area impinging on the sample, thereby increasing the number density of photoexcited carriers excited within the sample. At different fluences, the fit values of τ_i and A_i also change, but no significant change is observed in τ_r. [38].

Chapter 5

Simulation

Ultrafast pump probe methodology measures the differential transmission and reflection of materials as a function of the pump wavelength, laser fluence, and delay time. The difference in the behaviour occurs due to changes induced in the dielectric constant of the medium. The transmission and reflection of a given medium are directly related to the dielectric constant [16].

$$\begin{aligned} R &= \left|\frac{\sqrt{\epsilon_2}-\sqrt{\epsilon_1}}{\sqrt{\epsilon_2}+\sqrt{\epsilon_1}}\right|^2 \\ T &= \frac{4\sqrt{\epsilon_1}\sqrt{\epsilon_2}}{(\sqrt{\epsilon_1}+\sqrt{\epsilon_2})^2} \end{aligned} \tag{5.1}$$

The complex intraband (Drude) and interband dielectric constant spectra are calculated using models that take into account the band energy, size, and the plasma frequency of the material. The electron-lattice two temperature model is then used to calculate the extinction coefficient of the material as a function of delay time between the pump and probe. The simulations accurately depict the behaviour of the absorption versus time delay plot as well as the changes that occur by varying the pump wavelength and fluence [39][40][41][42][43][44][45].

5.1 Model

Laser heating of the sample initially gives rise to a non-Fermi distribution of electron, which quickly becomes a Fermi distribution after electron-electron thermalization process[39]. The time-scale for the electron-electron thermalization process is tens of femtoseconds[39]. Due to the smallness of the timescale, the electron-electron thermalization is ignored in the model and the electron is assumed to be Fermi distributed from the beginning.

The electron temperature starts decreasing by shedding its energy to the lattice by electron-phonon scattering. This process is modelled by a two temperature model for the electron and lattice. The electron specific heat is a linear function of electron temperature whereas the lattice specific heat constant is treated as a constant. The electron-phonon coupling constant is also treated as a constant throughout the process. Once the temperature profiles for the electron and lattice temperatures are obtained, the results are combined with the results from the absorption versus temperature spectrum obtained before to generate the ultrafast pump probe transient absorption spectrum for the nanoparticle [39][42].

5.1.1 Absorption spectrum

The absorption spectrum is calculated by the Mie expression for the absorption cross section of nanoparticles [46]:

$$\sigma(\omega, T) \propto \epsilon_m^{3/2} \frac{\omega \epsilon_2(\omega, T)}{[\epsilon_1(\omega, T) + 2\epsilon_m]^2 + \epsilon_2(\omega, T)^2} \tag{5.2}$$

and the transient signal is obtained by calculating the change in absorption spectrum [39]:

$$\Delta\sigma(\omega, T_e) = \sigma(\omega, T_e) - \sigma(\omega, T_e = 298K) \tag{5.3}$$

Here, ϵ_m is the dielectric constant of the surrounding medium. For this model, water ($\epsilon_m = 1.77$) was considered. ${}_1(\omega, T)$ and $\epsilon_2(\omega, T)$ are the real and complex dielectric spectra of the nanoparticle. For noble metals such as gold and silver, the dielectric constants are made up of the intraband, free-electron (Drude) contribution and interband transition contributions [39][42].

$$\begin{aligned} \epsilon_1(\omega, T) &= \epsilon_1^D(\omega) + \epsilon_1^{ib}(\omega, T) \\ \epsilon_2(\omega, T) &= \epsilon_2^D(\omega) + \epsilon_2^{ib}(\omega, T) \end{aligned} \tag{5.4}$$

The free electron contribution is given by [39][42]:

$$\begin{aligned} \epsilon_1^D &= 1 - \frac{\omega_p^2}{\omega^2 + \Gamma^2} \\ \epsilon_2^D &= \frac{\omega_p^2 \Gamma}{\omega(\omega^2 + \Gamma^2)} \end{aligned} \tag{5.5}$$

where ω_P is the plasma frequency ($1.36 \times 10^{16} radHz$) and Γ is the damping constant of the material. The damping constant of a nanoparticle is different from that of the bulk material. The expression for damping constant of a nanoparticle is given by [39]:

$$\Gamma = \Gamma_{bulk} + A\frac{V_F}{R} \tag{5.6}$$

where V_F is the Fermi velocity ($1.4 \times 10^6 ms^{-1}$ [47]), Γ_{bulk} is the damping constant of the bulk material (1.09×10^{14} [43]) and R is the radius of the nanoparticle. A is a constant parameter and it depends upon the electron-surface scattering model chosen. In this model, the value of A was chosen to be 2. [43].

The interband contribution to ϵ_2 is given by [42]:

$$\epsilon_2^{ib}(\omega, T) \propto \frac{\pi e^2}{3\epsilon_0 m_e^2 \omega^2} \int_0^\infty D(E, \omega)[1 - n(E, T)]dE \tag{5.7}$$

where $n(E, T)$ is the Fermi distribution function, $\varepsilon^{-3/2} \approx (2\pi/\hbar^3)m_e^{3/2}$ and $D(E, \omega)$ is known as the energy distribution of the joint density of states (EDJDOS). It has been shown that [48] [42]:

$$D(E, \omega) \propto \frac{\varepsilon^{-3/2}\sqrt{v_d}}{8\pi^2} \frac{\Theta[v_d\hbar(\omega - \omega_{ib}) - E]}{\sqrt{v_d\hbar(\omega - \omega_{ib}) - E}} \tag{5.8}$$

Θ is the Heaviside step function. v_d is a parameter whose value depends on the masses of charge carriers in the valence and conduction bands. Its value was taken as 0.92 [39]. ω_{ib} is the interband transition frequency and its value is 5.94×10^{15} [39].

The interband contribution to the real part of the dielectric constant is given by the Kramers-Kronig analysis of ϵ_2^{ib} [39]:

$$\epsilon_1^{ib} = \frac{2}{\pi} P \int_0^\infty \frac{\omega' \epsilon_2^{ib}(\omega', T)}{\omega'^2 - \omega^2} d\omega' \tag{5.9}$$

where P stands for the principal value of the integral.

All the contributions have now been obtained to calculate the dielectric constant spectrum. Optionally, one can add a multiplicative factor to the interband contribution in order to match the actual dielectric constant value. The spectrum is finally calculated using the first equation above.

In the case of nanorods (with semi-major and semi-minor axes a and b, respectively), the same procedure is followed except for a few changes in the formulae.

The damping constant for nanorods is given by [43]:

$$\Gamma = \Gamma_{bulk} + A\frac{V_F}{b} \tag{5.10}$$

A geometrical factor is introduced in the expression for extinction coefficient [46].

$$\sigma(\omega, T) \propto \epsilon_m^{3/2} \frac{\omega\epsilon_2(\omega, T)}{[\epsilon_1(\omega, T) + ((1 - L_i)/L_i)\epsilon_m]^2 + \epsilon_2(\omega, T)^2} \tag{5.11}$$

The factor depends on the light polarization and particle dimensions. For a nanorod with eccentricity $e^2 = 1 - (b/a)^2$ and light polarization parallel to its long (x) axis:

$$L_x = \frac{1 - e^2}{e^2}\Big[-1 + \frac{1}{2e}\ln\Big(\frac{1 + e}{1 - e}\Big)\Big] \tag{5.12}$$

whereas $L_y = L_z = (1 - L_x)/2$. For unpolarized light, a weighted sum of extinction coefficients implementing each of the geometric factors is used. For nanoparticles, $L_i = 1/3$ regardless of the incident polarization of light.

5.1.2 Two Temperature Model

The electron-phonon thermalization process is modelled by considering the electrons in thermal equilibrium at temperature $T_e(t)$ losing energy to the lattice phonons in thermal equilibrium at temperature $T_l(t)$.

$$\begin{aligned} C_e(T_e)\tfrac{dT_e}{dt} &= -g(T_e - T_l) \\ C_l\tfrac{dT_l}{dt} &= g(T_e - T_l) \end{aligned} \tag{5.13}$$

where C_e and C_l are the electron and lattice specific heats, respectively. g is the electron-phonon coupling constant. Their values are:

$$\begin{aligned} C_e(T_e) &= \alpha T_e \\ C_l &= 2.4 \times 10^6 JK^{-1}m^{-3} \\ g &= 3.5 \times 10^{16} Wm^{-3}K^{-1} \end{aligned} \tag{5.14}$$

where $\alpha = 65 Jm^{-3}K^{-2}$.

The initial electron temperature depends on the pump wavelength and fluence. The transient absorption of the sample is experimentally obtained and matched with the plot of transient absorption versus temperature at the specific pump frequency (which can be obtained using the calculations mentioned in the previous section) to determine the initial electron temperature. The initial lattice temperature is $298K$.

5.2 Results

The simulation was performed for silver nanoparticles of diameter 12 nm and silver nanorods of size 43x12 nm. The absorbance versus delay time behaviour was plotted by varying the pump wavelength away from the SPR resonance wavelength and also by changing the pump fluence. The results are shown in the figures below. All the constant values were in electron volt units, in order to make the computation feasible. The simulation was implemented using MATLAB and plotted using gnuplot. The full MATLAB code is provided in Appendix A

The decay times varying haphazardly with particle size in figure 5.8 should not come as a shock, since the localized surface plasmon resonance wavelength varies with particle size[39] and with pump wavelength (figures 5.3 and 5.4). In this simulation, the surface plasmon wavelength was not calculated for each particle. The proper way to compare the decay times for different particles would be to illuminate them at the surface plasmon wavelength and normalize with respect to the absorbance peak.

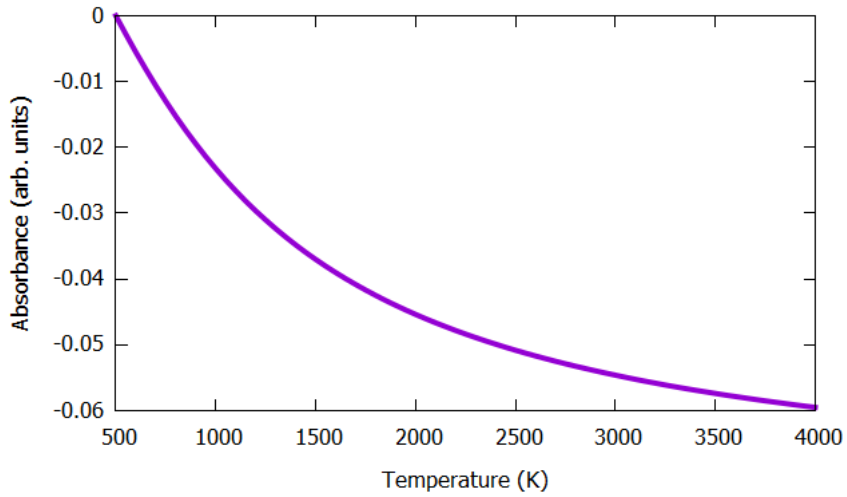

Figure 5.1: Absorbance versus temperature behaviour in a silver nanoparticle of diameter 12 nm. As expected, the absorbance value decreases as temperature. The pump wavelength for this calculation is 300 nm.

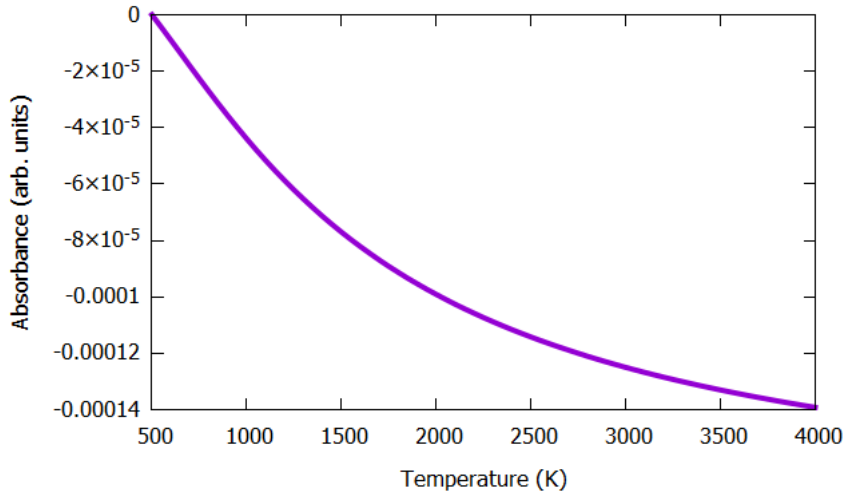

Figure 5.2: Absorbance versus temperature behaviour in a 43 $\times$ 12 nm nanorod. The pump wavelength for this calculation is 300 nm. The behaviour is similar to that of the nanoparticle.

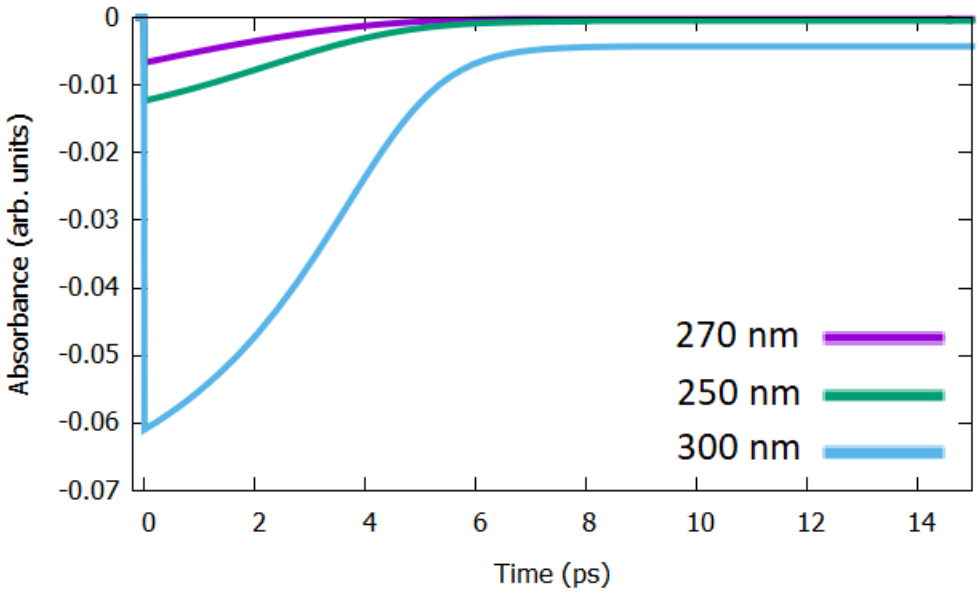

Figure 5.3: Absorbance versus pump-probe delay time of 12 nm silver nanoparticle at different pump wavelengths. There is an increase in the absolute value of the peak when the wavelength is reduced. However, there seems to be no effect on the decay time of the nanoparticle as per the design of the model.

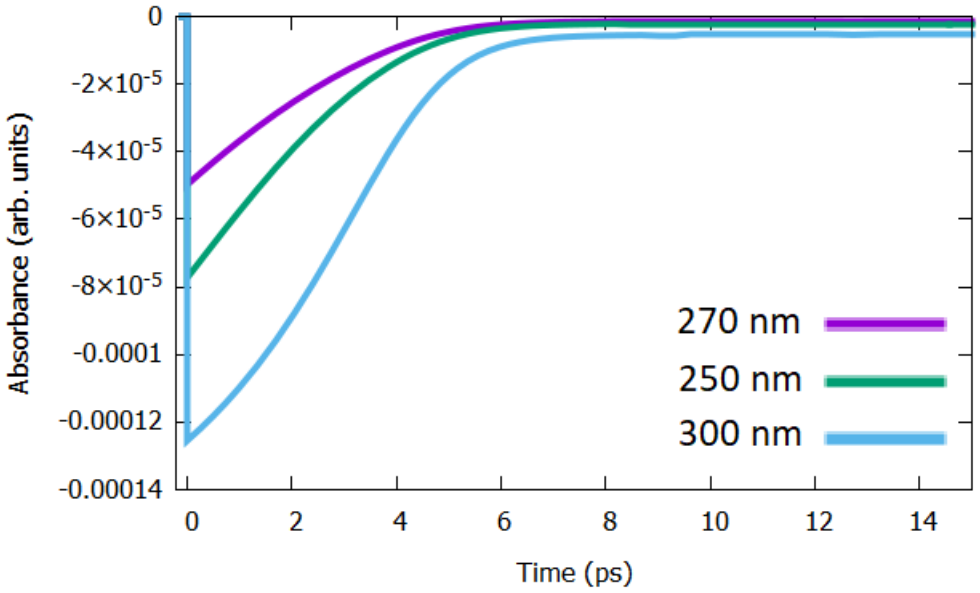

Figure 5.4: Absorbance versus pump-probe delay time of silver nanorod at different pump wavelengths. The behaviour is similar to that of the nanoparticle.

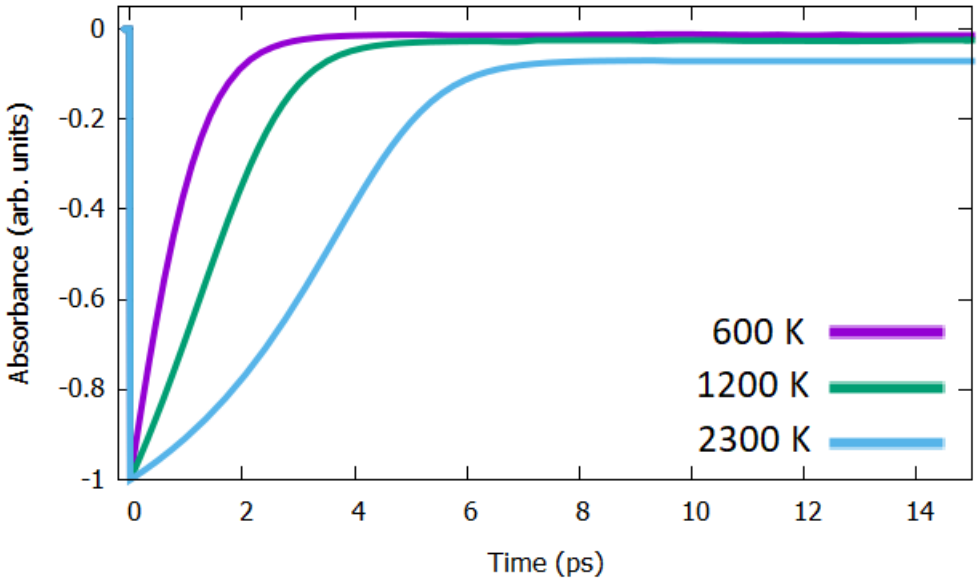

Figure 5.5: Normalized absorbance versus pump probe delay time of 12 nm silver nanoparticle at different pump fluences (initial electron temperatures). At lower fluences, a faster decay is predicted. The pump wavelength for this calculation is 300 nm.

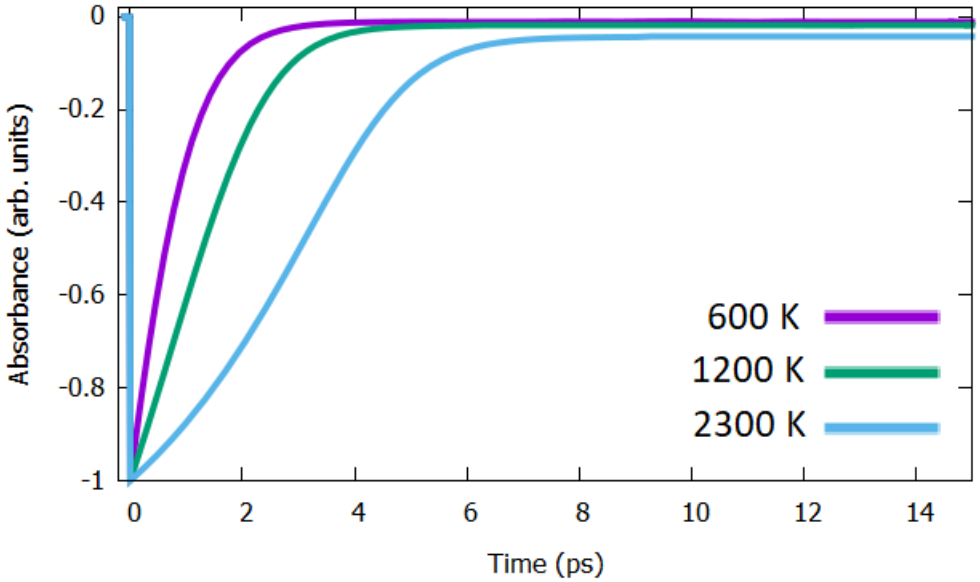

Figure 5.6: Absorbance versus pump-probe delay time of 12 nm silver nanorod at different pump fluences. The pump wavelength for this calculation is 300 nm. The behaviour is similar to that of the nanoparticle.

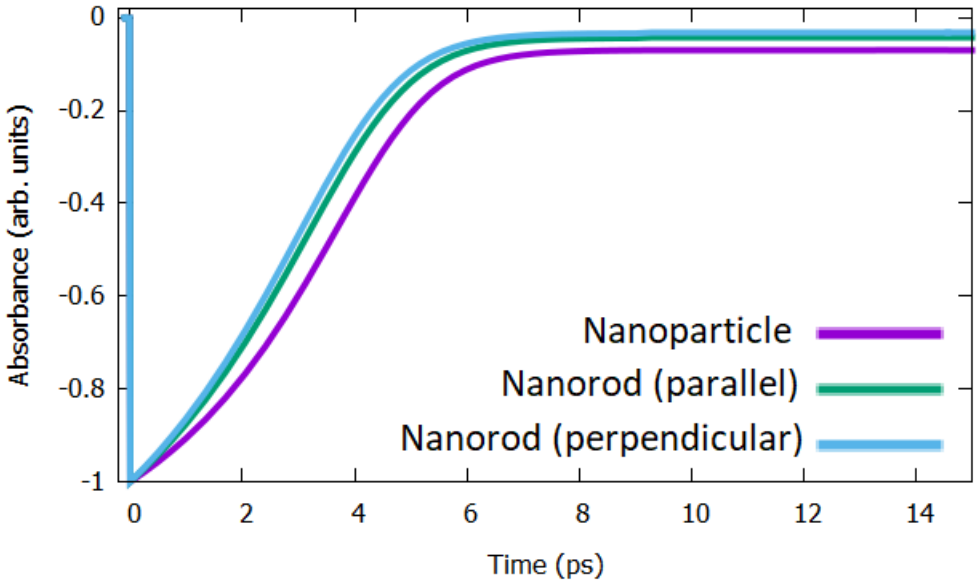

Figure 5.7: A comparison of the decay times of nanoparticle, nanorod with parallelly polarized light and nanorod with perpendicularly polarized light. The pump wavelength for this calculation is 300 nm and the intial electron temperature is 2300 K. A slight variation in the decay time is observed. The nanoparticle seems to decay the slowest while the nanorod illuminated with light polarized perpendicular to its long axis decays the fastest.

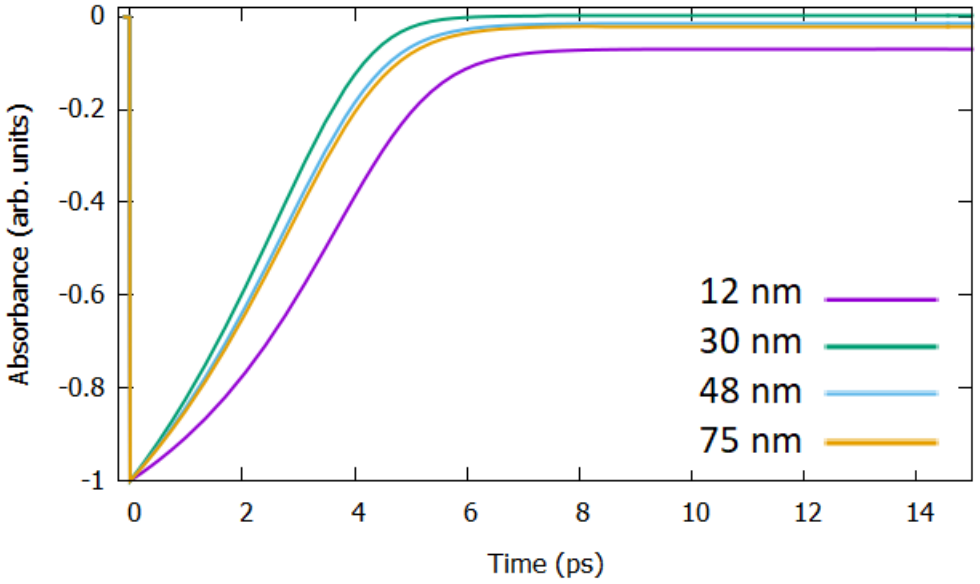

Figure 5.8: A comparison of the decay times of nanoparticles of different sizes. There seems to be no clear increasing or decreasing relationship. The pump wavelength for this calculation is 300 nm and the intial electron temperature is 2300 K.

Chapter 6

Transmitted Light Microscopy

The single-beam transmitted light microscopy study was performed on powder MoS_2. The setup consists of a single laser beam falling on the sample placed on a motorized XY stage. The transmitted beam from the sample is collected into a CCD where its intensity is recorded. The XY stage is translated in order to expose a different part of the sample. Transmittance as a function of x and y positions can be plotted to visualize the optical density of the sample at each point.

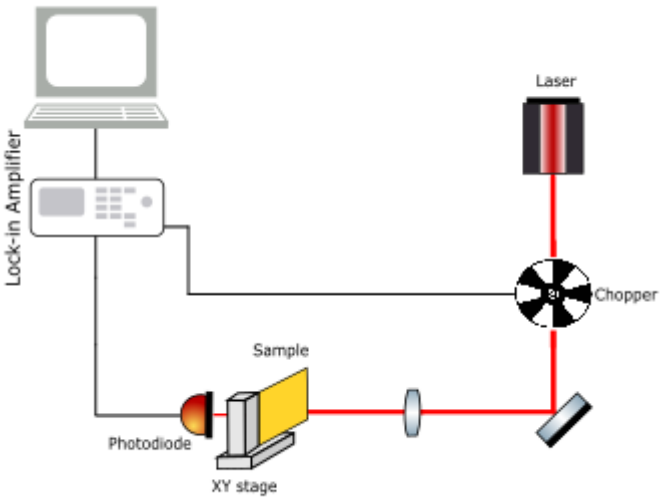

Figure 6.1: Setup for optical transmission microscopy of MoS_2 powder

The black MoS_2 powder was carefully spread out by hand on a glass slide such that monolayer covering was achieved to the maximum degree. The laser spot size for scanning was $25\mu m$. A square area within the sample of side length $0.5mm$ was chosen to study. The step lengths were equal to 0.01

mm and 0.025 mm for x and y scan, respectively. The differential transmission data was obtained for the square area and plotted.

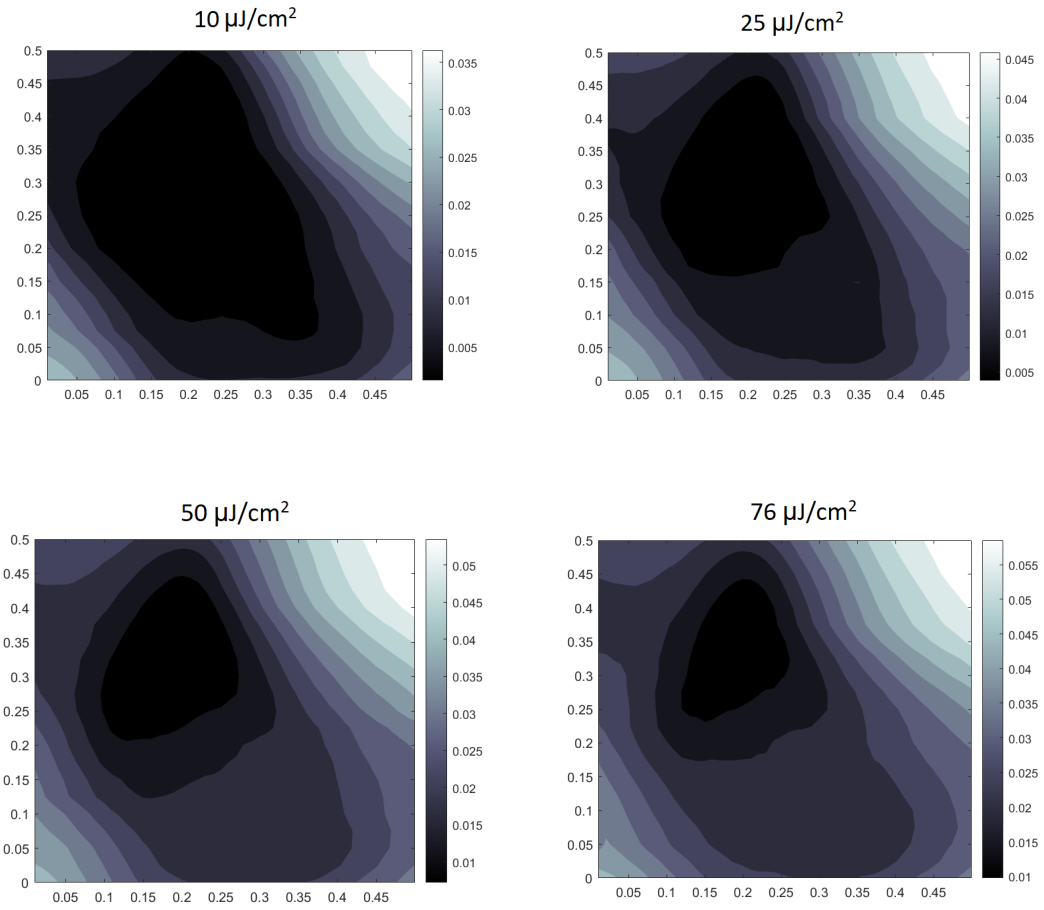

Figure 6.2: Results from scanning a square shaped area of the sample at four different fluences. An increase in transmission is observed as the fluence is increased.

The figures show that when the density of the MoS_2 powder is higher at a given spot, the transmission is lower and vice versa. The figures also indicate that the transmission increases with the laser power impinging on the sample.

Chapter 7

Conclusion

In addition to the experiment proposed in Chapter 4, the author would like the suggest a few modifications for future research.

1. The pump and probe spot size could be vastly smaller compared to the ones obtained above. Given the nanowire diameter, a smaller probe spot size would improve the quality of the output signal. A beam expansion setup was currently used to carry it out, but the improvement was meager.

2. Performing ultrafast pump probe spectroscopy on an ensemble of nanowires is useful for distinguishing the characteristics of a single nanowire, also if reducing the spot size is deemed practically impossible.

3. Ultrafast pump probe studies have been performed on bent semiconductor nanowires [49] [50]. It could be interesting to perform pump probe spectroscopy on bent and end-to-end connected metal nanowires.

4. Spatially separated pump probe spectroscopy studies have been reported in silicon nanowires [51]. The same could be performed for single/bent/connected metal nanorods.

The unfortunate timing of the start of the simulation forced the author to stop the simulations study mid way. The full code with the working and non-working parts has been provided in Appendix A. The author would like to point out the errors in the code and suggest a few improvements to the study:

1. The calculation to obtain the surface plasmon resonant wavelength of nanoparticles could not be performed by the author due to errors thrown by the code. The study of changing decay times is incomplete without calculating the SPR wavelength of the nanoparticles.

2. The plot of $\Delta\sigma$ versus λ could not be obtained as well due to errors thrown by the program. The author was unable to complete this section of the code.

3. The scope of the simulation could be expanded to cover gold nanostructures as well. A comparative study could be performed between the nanostructures of gold and silver.

4. Once the experimental data is obtained, the parameters used for the simulation could be modified to fit the actual data better.

Appendix A

MATLAB code for simulation

```
%Constants
eV2J = 1.6e-19;
h = 4.4e-15;
hbar = h/(2*pi);
eps0 = 8.85e-12;
echarge = 1.6e-19;
me = 0.511e6;
kb = 8.62e-5;
c = 3e8;
eps_m = 1.77;

%Particle characteristics
semi_major_axis = 43e-9/2;
semi_minor_axis = 12e-9/2;
econst = 2*me^(3/2)/(hbar^3);
A = 2;
v_f = 1.4e6;
tau_b = 9.1e-15;
Gamma_b = 1/tau_b;
Gamma = Gamma_b + A*v_f/semi_minor_axis;
omega_p = 1.36e16;
omega_ib = 3.9*eV2J/(6.6e-34/(2*pi));
vd = 0.92;
ecc = sqrt(1-(semi_minor_axis/semi_major_axis)^2);
Lx = ((1-ecc^2)/ecc^2)*(-1+log((1+ecc)/(1-ecc))/(2*ecc));
Ly = (1-Lx)/2;
Lz = (1-Lx)/2;
```

```
%Functions
syms E T omega omega_prime;
n(E,T) = 1/(1+exp(-E/(kb*T)));
D(E,omega) = econst*sqrt(vd)*heaviside(vd*hbar*(omega-omega_ib)-E)
                        /(8*pi^2*sqrt(vd*hbar*(omega-omega_ib)-E));
e1D(omega) = 1-omega_p^2/(omega^2+Gamma^2);
e2D(omega) = omega_p^2*Gamma/(omega*(omega^2+Gamma^2));
e2ib(omega,T) = (pi*echarge^2/(3*eps0*me^2*omega^2))
                        *vpaintegral(D(E,omega)*(1-n(E,T)),E,0,inf);
f1(omega_prime,omega,T) = omega_prime*e2ib(omega_prime,T)/
                                (omega_prime^2-omega^2)*2/pi;
dh = 1;
part1(omega,T) = vpaintegral(f1,omega_prime,0,omega-dh);
part2(omega,T) = vpaintegral(f1,omega_prime,omega+dh,inf);
e1ib(omega,T) = part1(omega,T)+part2(omega,T);

%Real and imaginary dielectric constants
e1(omega,T) = e1D(omega) + e1ib(omega,T);
e2(omega,T) = e2D(omega) + e2ib(omega,T);

%Mie Theory absorption cross section calculation
sigma(omega,T) = eps_m^(3/2)*omega*e2(omega,T)/
                        ((e1(omega,T)+((1-Ly)/Ly)*eps_m)^2+e2(omega,T)^2);

%Trial values
om = 2*pi*c/300e-9;
T1 = 500;
T0 = 298;
sigma(om,T0)
sigma(om,T1)

%To obtain the spectrum sigma versus wavelength
lams = 200e-9:1e-9:800e-9;
oms = 2*pi*c./lams;
sigs_T0 = [];
sigs_T1 = [];
for i = 1:length(lams)
    sigs_T0 = [sigs_T0, sigma(oms(i),T0)];
```

```
    sigs_T1 = [sigs_T1, sigma(oms(i),T1)];
    disp(i);
    disp(sigs_T0(i));
end
plot(lams/1e-9,(sigs_T1-sigs_T0)/max(sigs_T0));

%To find the SPR wavelength
func = @(x) x-(2*pi*c/omega_p)*sqrt(e1ib(2*pi*c/x,298)+2*eps_m);
x0 = 500e-9;
spr_lam = fzero(func,x0);

%Two temperature model
TeTl0 = [2300 298];
tspan = [0 50e-12];
[t,TeTl] = ode45(@(t,TeTl) ttmfn(t,TeTl),tspan,TeTl0);
plot(t,TeTl(:,1))

%To obtain the absorbance versus delay time plot
sig_fin = [];
lam0 = 300e-9;
om0 = 2*pi*c/lam0;
for i = (1:length(t))
    sig_fin = [sig_fin, sigma(om0,TeTl(i,1))];
    disp(i);
    disp(sig_fin(i));
end
sig_fin0 = sigma(om0,298);
plot(t/1e-12,-(sig_fin-sig_fin0));

%To obtain the plot of sigma versus temperature
Ts = 500:50:4000;
omT = 2*pi*c/300e-9;
sig_Ts = [];
for i = (1:length(Ts))
    sig_Ts = [sig_Ts, sigma(omT,Ts(i))];
    disp(i);
    disp(sig_Ts(i));
end
```

```
sig_Ts0 = max(sig_Ts);
plot(Ts,-(sig_Ts-sig_Ts0)-max(-(sig_Ts-sig_Ts0)));
```

References

[1] Orazio Svelto. *Principles of Lasers*. en. Boston, MA: Springer US, 2010. ISBN: 978-1-4419-1301-2 978-1-4419-1302-9. DOI: 10.1007/978-1-4419-1302-9. URL: http://link.springer.com/10.1007/978-1-4419-1302-9.

[2] Thomas Gaumnitz et al. "Streaking of 43-attosecond soft-X-ray pulses generated by a passively CEP-stable mid-infrared driver". en. In: *Opt. Express* 25.22 (Oct. 2017), p. 27506. ISSN: 1094-4087. DOI: 10.1364/OE.25.027506. URL: https://www.osapublishing.org/abstract.cfm?URI=oe-25-22-27506.

[3] Abdelaziz Boulesbaa et al. "Ultrafast Dynamics of Metal Plasmons Induced by 2D Semiconductor Excitons in Hybrid Nanostructure Arrays". en. In: *ACS Photonics* 3.12 (Dec. 2016), pp. 2389–2395. ISSN: 2330-4022, 2330-4022. DOI: 10.1021/acsphotonics.6b00618. URL: https://pubs.acs.org/doi/10.1021/acsphotonics.6b00618.

[4] Jagdeep Shah. "Ultrafast studies of carrier relaxation in semiconductors and their microstructures". en. In: *Superlattices and Microstructures* 6.3 (Jan. 1989), pp. 293–302. ISSN: 07496036. DOI: 10.1016/0749-6036(89)90172-9. URL: https://linkinghub.elsevier.com/retrieve/pii/0749603689901729.

[5] Rohit P. Prasankumar, Prashanth C. Upadhya, and Antoinette J. Taylor. "Ultrafast carrier dynamics in semiconductor nanowires". en. In: *Phys. Status Solidi (b)* 246.9 (Sept. 2009), pp. 1973–1995. ISSN: 03701972, 15213951. DOI: 10.1002/pssb.200945128. URL: http://doi.wiley.com/10.1002/pssb.200945128.

[6] Todd D. Krauss and Frank W. Wise. "Coherent Acoustic Phonons in a Semiconductor Quantum Dot". en. In: *Phys. Rev. Lett.* 79.25 (Dec. 1997), pp. 5102–5105. ISSN: 0031-9007, 1079-7114. DOI: 10.1103/PhysRevLett.79.5102. URL: https://link.aps.org/doi/10.1103/PhysRevLett.79.5102.

[7] V. Klimov, P. Haring Bolivar, and H. Kurz. "Ultrafast carrier dynamics in semiconductor quantum dots". en. In: *Phys. Rev. B* 53.3 (Jan. 1996),

pp. 1463–1467. ISSN: 0163-1829, 1095-3795. DOI: 10.1103/PhysRevB.53.1463. URL: https://link.aps.org/doi/10.1103/PhysRevB.53.1463.

[8] U. Kreibig and C. v. Fragstein. "The limitation of electron mean free path in small silver particles". en. In: *Z. Physik* 224.4 (Aug. 1969), pp. 307–323. ISSN: 1434-6001, 1434-601X. DOI: 10.1007/BF01393059. URL: http://link.springer.com/10.1007/BF01393059.

[9] U. Kreibig. "Kramers Kronig analysis of the optical properties of small silver particles". en. In: *Z. Physik* 234.4 (Aug. 1970), pp. 307–318. ISSN: 1434-6001, 1434-601X. DOI: 10.1007/BF01394718. URL: http://link.springer.com/10.1007/BF01394718.

[10] Chuanbo Gao et al. "Templated Synthesis of Metal Nanorods in Silica Nanotubes". en. In: *J. Am. Chem. Soc.* 133.49 (Dec. 2011), pp. 19706–19709. ISSN: 0002-7863, 1520-5126. DOI: 10.1021/ja209647d. URL: https://pubs.acs.org/doi/10.1021/ja209647d.

[11] Eleonora Petryayeva and Ulrich J. Krull. "Localized surface plasmon resonance: Nanostructures, bioassays and biosensing—A review". en. In: *Analytica Chimica Acta* 706.1 (Nov. 2011), pp. 8–24. ISSN: 00032670. DOI: 10.1016/j.aca.2011.08.020. URL: https://linkinghub.elsevier.com/retrieve/pii/S0003267011011196.

[12] ZhiYa Ma et al. "Applications of gold nanorods in biomedical imaging and related fields". en. In: *Chin. Sci. Bull.* 58.21 (July 2013), pp. 2530–2536. ISSN: 1001-6538, 1861-9541. DOI: 10.1007/s11434-013-5720-7. URL: http://link.springer.com/10.1007/s11434-013-5720-7.

[13] Paresh Chandra Ray. "Size and Shape Dependent Second Order Nonlinear Optical Properties of Nanomaterials and Their Application in Biological and Chemical Sensing". en. In: *Chem. Rev.* 110.9 (Sept. 2010), pp. 5332–5365. ISSN: 0009-2665, 1520-6890. DOI: 10.1021/cr900335q. URL: https://pubs.acs.org/doi/10.1021/cr900335q.

[14] Inci Donmez Noyan et al. "SiGe nanowire arrays based thermoelectric microgenerator". en. In: *Nano Energy* 57 (Mar. 2019), pp. 492–499. ISSN: 22112855. DOI: 10.1016/j.nanoen.2018.12.050. URL: https://linkinghub.elsevier.com/retrieve/pii/S2211285518309637.

[15] Jonathan E. Green et al. "A 160-kilobit molecular electronic memory patterned at 1011 bits per square centimetre". en. In: *Nature* 445.7126 (Jan. 2007), pp. 414–417. ISSN: 0028-0836, 1476-4687. DOI: 10.1038/nature05462. URL: http://www.nature.com/articles/nature05462.

[16] Hecht E. *Optics*. 4th ed. AW, 2002. ISBN: 0321188780,9780321188786.

[17] Andrew Marc Weiner. *Ultrafast optics*. en. Wiley series in pure and applied optics. OCLC: ocn262882128. Hoboken, N.J: Wiley, 2009. ISBN: 978-0-471-41539-8.

[18] S Banerjee, A Dan, and D Chakravorty. "Review Synthesis of conducting nanowires". en. In: (), p. 11.

[19] John Singleton. *Band Theory and Electronic Properties of Solids*. 1st ed. Oxford Master Series in Physics. Oxford University Press, 2001. ISBN: 978-0198506447.

[20] Irene Geijselaers et al. "Radial band bending at wurtzite–zinc-blende–GaAs interfaces". en. In: *Nano Futures* 2.3 (June 2018), p. 035002. ISSN: 2399-1984. DOI: 10.1088/2399-1984/aac96c. URL: https://iopscience.iop.org/article/10.1088/2399-1984/aac96c.

[21] Noor S Mohammad. "Understanding quantum confinement in nanowires: basics, applications and possible laws". en. In: *J. Phys.: Condens. Matter* 26.42 (Oct. 2014), p. 423202. ISSN: 0953-8984, 1361-648X. DOI: 10.1088/0953-8984/26/42/423202. URL: https://iopscience.iop.org/article/10.1088/0953-8984/26/42/423202.

[22] Michael Nolan et al. "Silicon Nanowire Band Gap Modification". en. In: *Nano Lett.* 7.1 (Jan. 2007), pp. 34–38. ISSN: 1530-6984, 1530-6992. DOI: 10.1021/nl061888d. URL: https://pubs.acs.org/doi/10.1021/nl061888d.

[23] Shixiong Zhang et al. "Relative Influence of Surface States and Bulk Impurities on the Electrical Properties of Ge Nanowires". en. In: *Nano Lett.* 9.9 (Sept. 2009), pp. 3268–3274. ISSN: 1530-6984, 1530-6992. DOI: 10.1021/nl901548u. URL: https://pubs.acs.org/doi/10.1021/nl901548u.

[24] Rohit Chikkaraddy, Danveer Singh, and G. V. Pavan Kumar. "Plasmon assisted light propagation and Raman scattering hot-spot in end-to-end coupled silver nanowire pairs". en. In: *Appl. Phys. Lett.* 100.4 (Jan. 2012), p. 043108. ISSN: 0003-6951, 1077-3118. DOI: 10.1063/1.3679649. URL: http://aip.scitation.org/doi/10.1063/1.3679649.

[25] Adrian Agreda et al. "Spatial Distribution of the Nonlinear Photoluminescence in Au Nanowires". en. In: *ACS Photonics* 6.5 (May 2019), pp. 1240–1247. ISSN: 2330-4022, 2330-4022. DOI: 10.1021/acsphotonics.9b00181. URL: https://pubs.acs.org/doi/10.1021/acsphotonics.9b00181.

[26] Daniel A. Clayton et al. "Photoluminescence and Spectroelectrochemistry of Single Ag Nanowires". en. In: *ACS Nano* 4.4 (Apr. 2010), pp. 2363–

2373. ISSN: 1936-0851, 1936-086X. DOI: 10.1021/nn100102k. URL: https://pubs.acs.org/doi/10.1021/nn100102k.

[27] A. Alec Talin et al. "Correlation of growth temperature, photoluminescence, and resistivity in GaN nanowires". en. In: *Appl. Phys. Lett.* 92.9 (Mar. 2008), p. 093105. ISSN: 0003-6951, 1077-3118. DOI: 10.1063/1.2889941. URL: http://aip.scitation.org/doi/10.1063/1.2889941.

[28] Jifa Qi, Angela M. Belcher, and John M. White. "Spectroscopy of individual silicon nanowires". en. In: *Appl. Phys. Lett.* 82.16 (Apr. 2003), pp. 2616–2618. ISSN: 0003-6951, 1077-3118. DOI: 10.1063/1.1569982. URL: http://aip.scitation.org/doi/10.1063/1.1569982.

[29] Jit Sarkar et al. "Ultrafast Carrier Dynamics of Undoped and Ho $^{3+}$ -Doped -Bismuth Oxide Microrods". en. In: *J. Phys. Chem. C* 123.15 (Apr. 2019), pp. 10007–10012. ISSN: 1932-7447, 1932-7455. DOI: 10.1021/acs.jpcc.8b12514. URL: https://pubs.acs.org/doi/10.1021/acs.jpcc.8b12514.

[30] Junaidi et al. "Controlling Shapes and Sizes of Synthesis Silver Nanowires by Polyol Method using Polyvinyl Alcohol and Polyvinyl Pyrrolidone". en. In: *Indian Journal of Science and Technology* 10.27 (June 2017), pp. 1–8. ISSN: 0974-5645, 0974-6846. DOI: 10.17485/ijst/2017/v10i27/93895. URL: http://www.indjst.org/index.php/indjst/article/view/93895.

[31] William C. Cieslik and Kenneth J. Kaufmann. "Detection of ultrafast phenomena with streak cameras and PMTs". en. In: ed. by Hongxing Jiang, Kong-Thon F. Tsen, and Jin-Joo Song. San Jose, CA, Apr. 2001, pp. 154–165. DOI: 10.1117/12.424731. URL: http://proceedings.spiedigitallibrary.org/proceeding.aspx?articleid=902238.

[32] Kannatassen Appavoo and Matthew Y. Sfeir. "Enhanced broadband ultrafast detection of ultraviolet emission using optical Kerr gating". en. In: *Review of Scientific Instruments* 85.5 (May 2014), p. 055114. ISSN: 0034-6748, 1089-7623. DOI: 10.1063/1.4873475. URL: http://aip.scitation.org/doi/10.1063/1.4873475.

[33] Haik Chosrowjan, Seiji Taniguchi, and Fumio Tanaka. "Ultrafast fluorescence upconversion technique and its applications to proteins". en. In: *FEBS J* 282.16 (Aug. 2015), pp. 3003–3015. ISSN: 1742464X. DOI: 10.1111/febs.13180. URL: http://doi.wiley.com/10.1111/febs.13180.

[34] V. Shcheslavskiy et al. "Ultrafast time measurements by time-correlated single photon counting coupled with superconducting single photon detector". en. In: *Review of Scientific Instruments* 87.5 (May 2016), p. 053117.

ISSN: 0034-6748, 1089-7623. DOI: 10.1063/1.4948920. URL: http://aip.scitation.org/doi/10.1063/1.4948920.

[35] Mizuho Fushitani. "Applications of pump-probe spectroscopy". en. In: *Annu. Rep. Prog. Chem., Sect. C: Phys. Chem.* 104 (2008), p. 272. ISSN: 0260-1826, 1460-4787. DOI: 10.1039/b703983m. URL: http://xlink.rsc.org/?DOI=b703983m.

[36] Petrissa Eckle et al. "Attosecond angular streaking". en. In: *Nature Phys* 4.7 (July 2008), pp. 565–570. ISSN: 1745-2473, 1745-2481. DOI: 10.1038/nphys982. URL: http://www.nature.com/articles/nphys982.

[37] J. Mauritsson et al. "Attosecond Electron Spectroscopy Using a Novel Interferometric Pump-Probe Technique". en. In: *Phys. Rev. Lett.* 105.5 (July 2010), p. 053001. ISSN: 0031-9007, 1079-7114. DOI: 10.1103/PhysRevLett.105.053001. URL: https://link.aps.org/doi/10.1103/PhysRevLett.105.053001.

[38] Sunil Kumar et al. "Probing ultrafast carrier dynamics, nonlinear absorption and refraction in core–shell silicon nanowires". en. In: *Pramana - J Phys* 79.3 (Sept. 2012), pp. 471–481. ISSN: 0304-4289, 0973-7111. DOI: 10.1007/s12043-012-0337-y. URL: http://link.springer.com/10.1007/s12043-012-0337-y.

[39] José H. Hodak, Ignacio Martini, and Gregory V. Hartland. "Spectroscopy and Dynamics of Nanometer-Sized Noble Metal Particles". en. In: *J. Phys. Chem. B* 102.36 (Sept. 1998), pp. 6958–6967. ISSN: 1520-6106, 1520-5207. DOI: 10.1021/jp9809787. URL: https://pubs.acs.org/doi/10.1021/jp9809787.

[40] Jose H. Hodak, Arnim Henglein, and Gregory V. Hartland. "Size dependent properties of Au particles: Coherent excitation and dephasing of acoustic vibrational modes". en. In: *The Journal of Chemical Physics* 111.18 (Nov. 1999), pp. 8613–8621. ISSN: 0021-9606, 1089-7690. DOI: 10.1063/1.480202. URL: http://aip.scitation.org/doi/10.1063/1.480202.

[41] O Ekici et al. "Thermal analysis of gold nanorods heated with femtosecond laser pulses". en. In: *J. Phys. D: Appl. Phys.* 41.18 (Sept. 2008), p. 185501. ISSN: 0022-3727, 1361-6463. DOI: 10.1088/0022-3727/41/18/185501. URL: https://iopscience.iop.org/article/10.1088/0022-3727/41/18/185501.

[42] Andrea Marini et al. "Thermo-modulational interband susceptibility and ultrafast temporal dynamics in nonlinear gold-based plasmonic

devices". en. In: *arXiv:1208.1119 [physics]* (Aug. 2012). arXiv: 1208.1119. URL: http://arxiv.org/abs/1208.1119.

[43] Jagmeet Singh Sekhon and S. S. Verma. "Optimal Dimensions of Gold Nanorod for Plasmonic Nanosensors". en. In: *Plasmonics* 6.1 (Mar. 2011), pp. 163–169. ISSN: 1557-1955, 1557-1963. DOI: 10.1007/s11468-010-9182-3. URL: http://link.springer.com/10.1007/s11468-010-9182-3.

[44] Tatjana Stoll et al. "Advances in femto-nano-optics: ultrafast nonlinearity of metal nanoparticles". en. In: *Eur. Phys. J. B* 87.11 (Nov. 2014), p. 260. ISSN: 1434-6028, 1434-6036. DOI: 10.1140/epjb/e2014-50515-4. URL: http://link.springer.com/10.1140/epjb/e2014-50515-4.

[45] Honghua U. Yang et al. "Optical dielectric function of silver". en. In: *Phys. Rev. B* 91.23 (June 2015), p. 235137. ISSN: 1098-0121, 1550-235X. DOI: 10.1103/PhysRevB.91.235137. URL: https://link.aps.org/doi/10.1103/PhysRevB.91.235137.

[46] Vollmer M. Kreibig U. *Optical properties of metal clusters*. Springer Series in Materials Science. Springer, 1995. ISBN: 0387578366,9780387578361.

[47] Zhe Cheng et al. "Temperature Dependence of Electrical and Thermal Conduction in Single Silver Nanowire". en. In: *Sci Rep* 5.1 (Sept. 2015), p. 10718. ISSN: 2045-2322. DOI: 10.1038/srep10718. URL: http://www.nature.com/articles/srep10718.

[48] Rogier H. M. Groeneveld, Rudolf Sprik, and Ad Lagendijk. "Femtosecond spectroscopy of electron-electron and electron-phonon energy relaxation in Ag and Au". en. In: *Phys. Rev. B* 51.17 (May 1995), pp. 11433–11445. ISSN: 0163-1829, 1095-3795. DOI: 10.1103/PhysRevB.51.11433. URL: https://link.aps.org/doi/10.1103/PhysRevB.51.11433.

[49] M. A. Seo et al. "Understanding ultrafast carrier dynamics in single quasi-one-dimensional Si nanowires". en. In: *Appl. Phys. Lett.* 100.7 (Feb. 2012), p. 071104. ISSN: 0003-6951, 1077-3118. DOI: 10.1063/1.3685487. URL: http://aip.scitation.org/doi/10.1063/1.3685487.

[50] Erik M. Grumstrup et al. "Reversible Strain-Induced Electron–Hole Recombination in Silicon Nanowires Observed with Femtosecond Pump–Probe Microscopy". en. In: *Nano Lett.* 14.11 (Nov. 2014), pp. 6287–6292. ISSN: 1530-6984, 1530-6992. DOI: 10.1021/nl5026166. URL: https://pubs.acs.org/doi/10.1021/nl5026166.

[51] Erik M. Grumstrup et al. "Ultrafast Carrier Dynamics in Individual Silicon Nanowires: Characterization of Diameter-Dependent Carrier Lifetime and Surface Recombination with Pump–Probe Microscopy". en.

In: *J. Phys. Chem. C* 118.16 (Apr. 2014), pp. 8634–8640. ISSN: 1932-7447, 1932-7455. DOI: 10.1021/jp502737e. URL: https://pubs.acs.org/doi/10.1021/jp502737e.